blood®
Regular Article

PLATELETS AND THROMBOPOIESIS

CRLF3 plays a key role in the final stage of platelet genesis and is a potential therapeutic target for thrombocythemia

Cavan Bennett,[1] Moyra Lawrence,[1,2] Jose A. Guerrero,[1] Simon Stritt,[3] Amie K. Waller,[1,2] Yahui Yan,[4] Richard W. Mifsud,[4] Jose Ballester-Beltrán,[1] Ayesha Baig,[3] Annett Mueller,[1,2] Louisa Mayer,[1] James Warland,[1,2] Christopher J. Penkett,[1] Parsa Akbari,[5,6] Thomas Moreau,[1] Amanda L. Evans,[1,2] Souradip Mookerjee,[1,2] Gary J. Hoffman,[7] Kourosh Saeb-Parsy,[8] David J. Adams,[9] Amber L. Couzens,[10] Markus Bender,[3] Wendy N. Erber,[7] Bernhard Nieswandt,[3] Randy J. Read,[4] and Cedric Ghevaert[1,2]

[1]Department of Haematology, Cambridge Blood Centre, National Health Service Blood and Transplant, University of Cambridge, Cambridge, United Kingdom; [2]Jeffrey Cheah Biomedical Centre, Cambridge Stem Cell Institute, University of Cambridge, Cambridge, United Kingdom; [3]Institute of Experimental Biomedicine, University Hospital, University of Würzburg, Würzburg, Germany; [4]Department of Haematology, Cambridge Institute for Medical Research, University of Cambridge, Cambridge, United Kingdom; [5]Medical Research Council/British Heart Foundation Cardiovascular Epidemiology Unit, Strangeways Research Laboratory, Department of Public Health and Primary Care, University of Cambridge, Cambridge, United Kingdom; [6]Department of Human Genetics, Wellcome Trust Sanger Institute, Cambridge, United Kingdom; [7]Faculty of Health and Medical Sciences, Medical School, University of Western Australia, Crawley, WA, Australia; [8]Department of Surgery, NIHR Cambridge Biomedical Research Centre, University of Cambridge, Cambridge, United Kingdom; [9]Wellcome Trust Sanger Institute, Cambridge, United Kingdom; and [10]Lunenfeld-Tanenbaum Research Institute, Sinai Health System, Toronto, ON, Canada

KEY POINTS

- **CRLF3 deficiency causes an isolated and sustained reduction in platelet count in mice.**
- **CRLF3 is a potential therapeutic target for thrombocythemia.**

The process of platelet production has so far been understood to be a 2-stage process: megakaryocyte maturation from hematopoietic stem cells followed by proplatelet formation, with each phase regulating the peripheral blood platelet count. Proplatelet formation releases into the bloodstream beads-on-a-string preplatelets, which undergo fission into mature platelets. For the first time, we show that preplatelet maturation is a third, tightly regulated, critical process akin to cytokinesis that regulates platelet count. We show that deficiency in cytokine receptor-like factor 3 (CRLF3) in mice leads to an isolated and sustained 25% to 48% reduction in the platelet count without any effect on other blood cell lineages. We show that *Crlf3*$^{-/-}$ preplatelets have increased microtubule stability, possibly because of increased microtubule glutamylation via the interaction of CRLF3 with key members of the Hippo pathway. Using a mouse model of JAK2 V617F essential thrombocythemia, we show that a lack of CRLF3 leads to long-term lineage-specific normalization of the platelet count. We thereby postulate that targeting CRLF3 has therapeutic potential for treatment of thrombocythemia.

Introduction

Platelets are small (2-4 μm) anucleated blood cells, the main function of which is to form thrombi upon vessel injury. Thrombi can form inappropriately on atherothrombotic plaques, causing heart attacks or strokes. Platelets are produced by megakaryocytes (MKs), which derive from hematopoietic stem cells (HSCs). To release platelets, MKs produce long cytoskeletal processes (proplatelets), which extend into the circulation, where large fragments (preplatelets) are shed.[1,2] Preplatelets undergo fission to form mature discoid platelets.[3]

Thrombocytopenia (platelet count $<150 \times 10^9$/L) can be caused by lack of platelet production or peripheral consumption of platelets. Multiple genetic disorders affect platelet production, which can be broadly separated into 2 groups: disorders that affect MK differentiation (the first stage of platelet production) and disorders that affect proplatelet formation (the second stage). Unsurprisingly, mutations associated with the latter are often in genes associated with the actin-tubulin cytoskeleton, such as *TUBB1*,[4] *MHY9*,[5] *FLNA*,[6] *ACTN1*,[7] *TPM4*,[8] and *DIAPH1*.[9]

Thrombocythemia (platelet count $>450 \times 10^9$/L) resulting from acquired clonal mutations in HSCs is termed essential thrombocythemia (ET). The major mutations seen in ET affect the tyrosine kinase Janus kinase 2 (JAK2),[10-13] the endoplasmic reticulum chaperone calreticulin,[14,15] and the thrombopoietin (TPO) receptor MPL.[16,17] Patients with ET typically have high survival rates, and the main complications are serious thrombotic events (affecting one-third of patients). The therapeutic management in patients with ET is primarily to prevent thrombotic events[18] with agents that reduce platelet function (low-dose aspirin) and cytoreductive agents that reduce MK production (hydroxyurea and anagrelide).

Cytokine receptor-like factor 3 (CRLF3) is a poorly studied but widely expressed 488–amino acid protein encoded in chromosome 17q11.2 in a region that is deleted in neurofibromatosis

type 1. CRLF3 is implicated in cell-cycle progression by overexpression in cell lines.[19]

We show for the first time that preplatelet fission to platelets is a critical rate-limiting step of platelet production (the third stage) and that CRLF3 plays a central role in this process by controlling microtubule stability, potentially through its interaction with Hippo pathway proteins. We also show that CRLF3 deficiency leads to isolated and sustained correction of platelet count in a mouse model of ET, showing its potential as a novel therapeutic target for ET.

Methods

Ethics

This research was regulated by the UK Animals (Scientific Procedures) Act 1986 Amendment Regulations 2012 (project license 70/8406) and the district government of Lower Franconia (Bezirksregierung Unterfranken). Human blood samples were obtained from healthy volunteers under local ethics approval (HBREC.2018.13). Ethical approval for whole-genome sequencing was provided by the East of England Cambridge South national research ethics committee (13/EE/0325). Informed consent was obtained as per the Declaration of Helsinki.

Animals

Generation of *Crlf3*$^{-/-}$ (*Crlf3*$^{tm1b(KOMP)Wtsi}$) mice was performed as previously reported.[20-22] Mice were maintained on a C57Bl/6 background. Age- and sex-matched control animals were used in all experiments.

Complete blood counts

ETDA anticoagulated whole blood taken from the tail vein or inferior vena cava was run on an ABC blood counter (Woodley) or Vet abc Plus+ (Scil).

In vitro platelet assays

Platelet response to agonists,[23] platelet spreading,[24] expression of major platelet receptors,[25] platelet survival,[26] and cold-induced microtubule disassembly[9] were performed as previously described. Thrombus formation assays were performed with heparin anticoagulated whole blood flowed into Vena8 Fluoro+ Biochips (Cellix) precoated with HORM Collagen (Takeda) as described.[27] Five images per channel were obtained using an EVOS fl microscope and AMG camera and analyzed in ImageJ.

Platelet depletion

Mice were injected intraperitoneally with 0.6 μg/g of anti-CD42b (Emfret Analytics) in phosphate-buffered saline. Mice were bled for complete blood count from the tail vein at 0, 24, 48, 72, and 96 hours postinjection into EDTA-coated tubes (Microvette).

Splenectomy

Platelet and preplatelet counts were determined pre-/post-splenectomy by flow cytometry as described.[28] Preplatelets were counted as GPV^{+}/GPIIbIIIa^{+} events with larger forward/sideward scatter characteristics than platelets. Heparinized blood incubated with antibodies against activated GPIIbIIIa (M023-2) and CD62P (M130-1; both Emfret Analytics) eliminated preplatelets as microaggregates (supplemental Figure 4D, available on the *Blood* Web site).

Platelet imaging

Transmission and scanning electron microscopy, rapid Romanowsky staining, and confocal microscopy were performed as detailed in the data supplement. Two-photon intravital microscopy was performed as described.[29]

MK cultures

Mouse bone marrow (BM) cells were prepared, MKs cultured, and mature MKs purified as described.[23,30] Differentiation and ploidy of cultured MKs were analyzed as described[23] using propidium iodide (Sigma-Aldrich). Samples were acquired using a Beckman Coulter Cyan flow cytometer and analyzed using Kaluza Analysis (version 1.5a) software (Beckman Coulter). Details of in vitro proplatelet formation are provided in the data supplement.

iPSC MKs

Forward programming of tandem affinity purification (TAP)–tagged (data supplement) and untagged induced pluripotent stem cells (iPSCs) to iPSC MKs was performed as previously described.[27] Proplatelet formation was carried out as described. For protein distribution, iPSC MKs attached to coverslips were fixed with 10% neutral buffered formalin (Sigma-Aldrich) and stained with antibodies against α-tubulin (T5168), FLAG (F1804; both Sigma-Aldrich), and 4′,6-diamidino-2-phenylindole (DAPI). Images were acquired using a Leica Sp5 inverted confocal microscope with a 63× immersion oil objective and Leica LAS 2.1 software and analyzed using ImageJ.

Structural solution of CRLF3

Purified murine CRLF3 protein (amino acids 174-442) was obtained using standard cloning, production, and purification methods. Crystallization was screened by the vapor diffusion method in 96-well sitting drop plates set up with a Nanodrop Screenmaker 96 + 8 (Innovadyne Technologies). Diffraction data were recorded at Diamond Light Source (Didcot, United Kingdom). The structure was determined by Hg-SAD using the AutoSol-wizard[31] of the PHENIX suite[32] with a data set collected with a wavelength of 1.006 Å from a crystal grown in 20% PEG 3350 and 0.2 M sodium formate (pH, 7.0) and soaked with 10 mM of thimerosal (Sigma-Aldrich) for 16 hours. The structure was refined to a resolution of 1.61 Å using Phenix.refine[32] and by manual building in Coot.[33] Full methodology is provided in the data supplement.

Genome-wide association studies

We performed a genetic association analysis of 3 loci (MOB1A, CRLF3, and STK38) to test for associations with 29 hematological parameters with imputed variants of minor allele frequency (MAF) >0.005% and INFO score >0.4. A significance threshold of 8.31×10^{-9} identifies associated variants located in each of the 3 genes by annotation with a variant effect predictor. Furthermore, we performed a multiple stepwise regression analysis to identify the number conditionally independent variants representing independent association signals in each locus.

Genetic variants in the human population

The primary data were obtained by whole-genome sequencing from whole-blood DNA from 13 037 individuals in the National Institute for Health Research BioResourceRare Diseases and 100 000 Genomes Project Pilot studies.[34,35] Quality control,

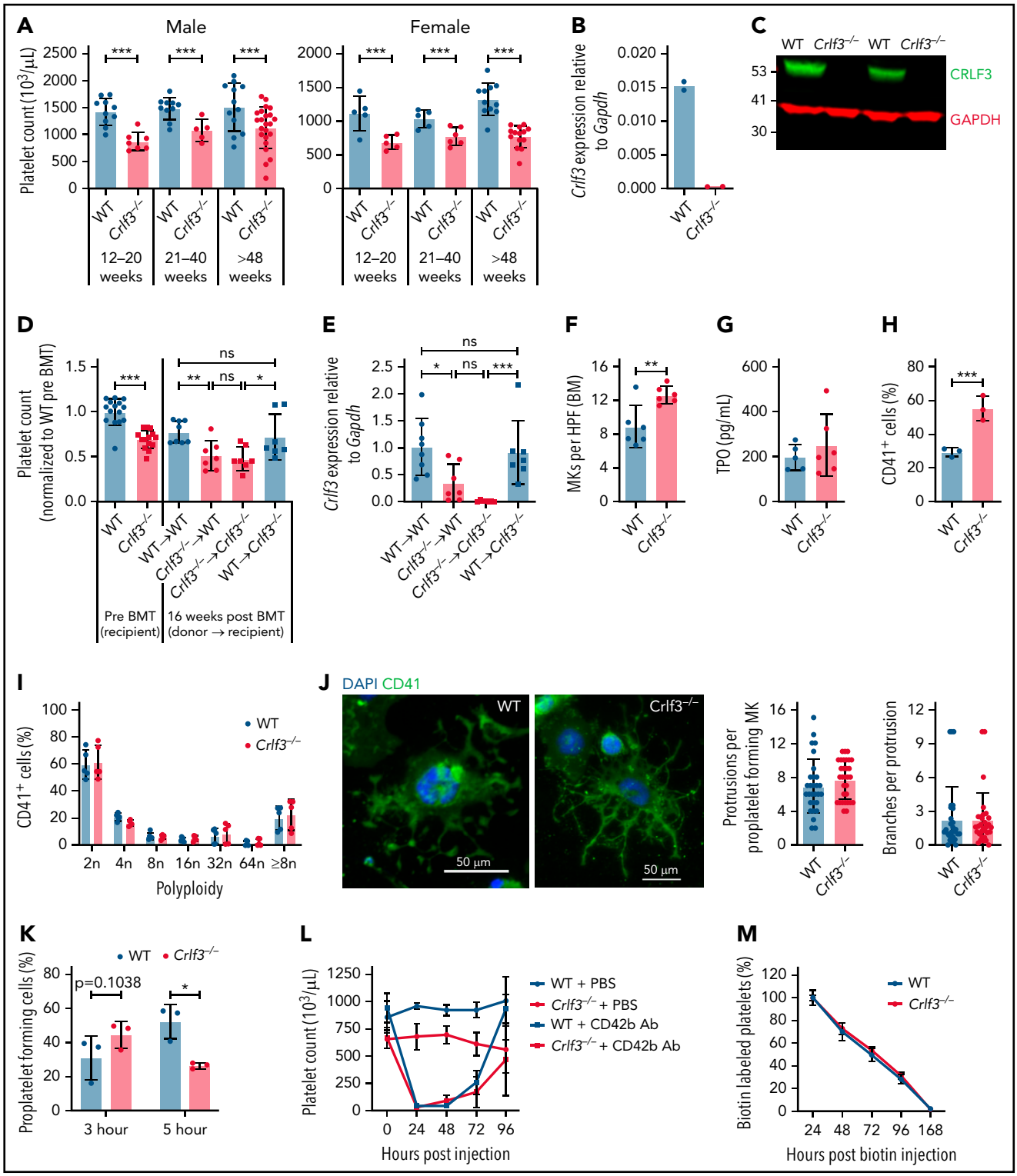

Figure 1. CRLF3 deficiency causes sustained and isolated reduction in platelet count. (A) Platelet counts of male (n = 5-23) and female (n = 5-14) young (12-20 weeks), middle aged (21-40 weeks), and old (>48 weeks) control (WT; blue) and *Crlf3*$^{-/-}$ (red) mice. (B) Expression of *Crlf3* relative to *Gapdh* messenger RNA (mRNA) determined by quantitative reverse transcription polymerase chain reaction (qRT-PCR) of control (WT; blue) and *Crlf3*$^{-/-}$ (red) isolated from in vitro cultured MKs (n = 2). (C) Western blot of platelet lysates against CRLF3 (green) and glyceraldehyde-3-phosphate dehydrogenase (GAPDH; red; n = 2). (D) Platelet counts pre- (left; n = 15 WT and 14 *Crlf3*$^{-/-}$) and 16 weeks post–BM transplantation (BMT; right) of control (WT; circles) and *Crlf3*$^{-/-}$ (squares) recipient mice that received either control (WT; blue) or *Crlf3*$^{-/-}$ (red) donor cells (n = 8 WT → WT; n = 7 all other groups). (E) Chimerism was estimated by expression of *Crlf3* relative to *Gapdh* mRNA isolated from in vitro cultured MKs by qRT-PCR (n = 8 WT → WT; 7 all other groups). (F) Quantification of MKs in hematoxylin and eosin–stained sections of control (WT; blue) and *Crlf3*$^{-/-}$ (red) tibias (n = 6). (G) TPO concentration determined by enzyme-linked immunosorbent assay in control (WT; blue) and *Crlf3*$^{-/-}$ (red) plasma (n = 5 WT and 6 *Crlf3*$^{-/-}$). (H) Percentage of CD41^{+} cells from control (WT; blue) and *Crlf3*$^{-/-}$ (red) in vitro MK cultures (n = 3). (I) Polyploidy of in vitro cultured control (WT; blue)

demographics, and variant calling are described in the report by Karczewski et al.[34]

Statistics

Sample sizes and statistical tests for each experiment are denoted in the figure legends (statistical testing was performed in Prism 8.0.1 [GraphPad Software]). A P value of $<.05$ was considered statistically significant ($*P < .05$, $**P < .01$, $***P < .005$). Data are presented as means ± standard deviations.

Additional methods used in this study are provided in the data supplement.

Results

Crlf3 deficiency causes an isolated reduction in platelet count

Crlf3$^{-/-}$ mice were generated as part of a genome-wide screening program,[20-22] leading to germ line deletion of *Crlf3* exon 2. Despite *Crlf3* being expressed in a large variety of tissues, including all hematopoietic lineages, *Crlf3*$^{-/-}$ animals show a sustained and isolated 25% to 48% reduction in platelet count ($P < .005$) compared with control (wild-type [WT]) animals (Figure 1A; supplemental Table 1), justifying further study of this mouse strain. *Crlf3* messenger RNA was significantly reduced in cultured MKs from *Crlf3*$^{-/-}$ animals (Figure 1B), and CRLF3 protein was undetectable in both *Crlf3*$^{-/-}$ cultured MK (Figure 1C) and platelet lysates (data not shown).

To assess whether the thrombocytopenia in *Crlf3*$^{-/-}$ animals was driven by factors intrinsic to the hematopoietic compartment, we performed BMTs. Control or *Crlf3*$^{-/-}$ BM cells were transplanted into irradiated control or *Crlf3*$^{-/-}$ recipient mice. Where donor and recipient genotypes were matched, the differences in platelet count determined pre-BMT remained true (Figure 1D). However, when WT recipients received *Crlf3*$^{-/-}$ BM, the platelet count post-BMT decreased to levels comparable to those in *Crlf3*$^{-/-}$ recipients that received *Crlf3*$^{-/-}$ BM ($P = .9965$). In contrast, when *Crlf3*$^{-/-}$ recipients received WT BM, the platelet count increased, reaching levels comparable to those in WT recipients that received WT BM ($P = .9650$). We confirmed that the posttransplantation platelet count correlated with *Crlf3* expression in cultured MKs derived from recipient BM samples (Figure 1E).

Next, we sought to clarify whether the thrombocytopenia was caused by decreased platelet production and/or increased platelet clearance. MK differentiation was preserved; *Crlf3*$^{-/-}$ mice had increased BM MKs (MKs per field, 12.65 ± 1.03 for *Crlf3*$^{-/-}$ vs 8.90 ± 2.51 for WT; $P = .0069$; Figure 1F; supplemental Figure 1), TPO concentrations were only marginally increased in *Crlf3*$^{-/-}$ mice (253 ± 136 vs 201 ± 56 pg/mL; $P = .4500$; Figure 1G), *Crlf3*$^{-/-}$ BM samples cultured in a suboptimal concentration of TPO showed a higher percentage of CD41^{+} cells after 5 days compared with controls (55.4% ± 7.1% vs 29.7% ± 2.5%; $P = .0042$; Figure 1H), and ploidy of cultured MKs was unchanged (Figure 1I). Proplatelet formation was morphologically similar between *Crlf3*$^{-/-}$ and control cultured MKs (Figure 1J), showing similar numbers of protrusions ($P = .2989$; Figure 1J, left panel) and branching ($P = .9226$; Figure 1J, right panel). However, proplatelet dynamics appeared altered between cultured MKs from *Crlf3*$^{-/-}$ and control animals. A greater proportion of *Crlf3*$^{-/-}$ MKs formed proplatelets 3 hours postseeding onto fibrinogen (45% ± 8% vs 31% ± 13%; $P = .1038$; Figure 1K; supplemental Figure 2), whereas at 5 hours, the trend was reversed (26% ± 2% vs 52% ± 10%; $P = .0164$). We presume the data at 5 hours reflect proplatelet-forming MKs seen at 3 hours in the *Crlf3*$^{-/-}$ sample having fragmented into platelets at 5 hours, which is supported by the reduced density of *Crlf3*$^{-/-}$ MKs at 5 hours (supplemental Figure 2). Using in vivo 2-photon intravital microscopy, we confirmed *Crlf3*$^{-/-}$ MKs formed long proplatelet protrusions into BM sinusoids, which appeared to be no different from those seen in control animals (supplemental Videos 1 and 2). Finally, we assessed platelet recovery after platelet depletion. Platelet counts in depleted *Crlf3*$^{-/-}$ and control animals recovered at an indistinguishable rate, with platelet counts reaching their respective values before depletion in 96 hours (Figure 1L). These data confirm that *Crlf3*$^{-/-}$ MKs differentiate normally and can produce platelets at least at a normal rate. The slight increase in MKs would imply a compensatory mechanism to increased platelet consumption.

We next considered whether the reduced platelet count was due to abnormal platelet function and/or clearance. *Crlf3*$^{-/-}$ mice do not display any overt bleeding phenotype. We carried out a tail bleeding assay, and 1 *Crlf3*$^{-/-}$ animal did show increased blood loss in the early time point compared with controls and its *Crlf3*$^{-/-}$ littermate upon tail transection (supplemental Figure 3A). We confirmed there were no gross differences in any main platelet functions, namely adhesion, spreading, activation, or thrombus formation. The expression of key platelet surface receptors/integrins was similar ($P > .05$ for all tested; supplemental Figure 3B). Platelet activation measured as fibrinogen binding and P-selectin surface expression by flow cytometry was comparable in response to different agonists ($P > .05$ for all agonists at all doses; supplemental Figure 3C). Platelet spreading onto fibrinogen was also not different ($P = .7717$;

Figure 1 (continued) and *Crlf3*$^{-/-}$ (red) MKs analyzed by flow cytometry (n = 5). (J) Mature in vitro cultured MKs were purified by bovine serum albumin gradient, seeded onto fibrinogen-coated coverslips and incubated at 37°C for 5 hours to induce proplatelet formation. Fixed samples were stained with CD41 (green) and DAPI (blue) and imaged by fluorescence microscopy. Images are representative of *Crlf3*$^{-/-}$ and control (WT) proplatelet-forming MKs. Scale bars are 50 μm. Proplatelet morphology of control (WT; blue) and *Crlf3*$^{-/-}$ (red) MKs was assessed by blindly quantifying the number of protrusions per proplatelet-forming MK and number of branches per protrusion (n = 29 WT and 31 *Crlf3*$^{-/-}$). (K) In vitro cultured MKs were seeded onto fibrinogen-coated coverslips and incubated at 37°C for 3 or 5 hours to induce proplatelet formation. After confocal microscopy, percentage of proplatelet forming MKs was determined for control (WT; blue) and *Crlf3*$^{-/-}$ (red; n = 3). At least 460 MKs were counted in each condition. (L) Control (WT; blue) and *Crlf3*$^{-/-}$ (red) animals were injected with phosphate-buffered saline (PBS; circles) or anti-CD42b (0.6 μg/g body weight; squares) and platelet counts determined by automated hemocytometer 0, 24, 48, 72, and 96 hours postinjection (n = 4 *Crlf3*$^{-/-}$ plus CD42b antibody [Ab]; n = 3 all other groups). (M) Control (WT; blue) and *Crlf3*$^{-/-}$ (red) mice were injected with 1 mg of NHS-biotin, and percentage of CD41^{+}/Ter119^{-}/streptavidin^{+} platelets was determined by flow cytometry at 24, 48, 72, 96, and 168 hours postinjection. Percentage of streptavidin^{+} platelets at 24 hours represents 100% biotin-bound platelets (n = 5). Data represent means ± standard deviations. Unpaired 2-tailed Student *t* test (F-H,J) with correction for multiple comparisons using the Holm-Sidak method (A), 1-way analysis of variance (ANOVA) (D,E), or 2-way ANOVA (I,K-M) with correction for multiple comparisons using the Holm-Sidak method. $*P < .05$, $**P < .01$, $***P < .005$. HPF, high-powered field; ns, not significant.

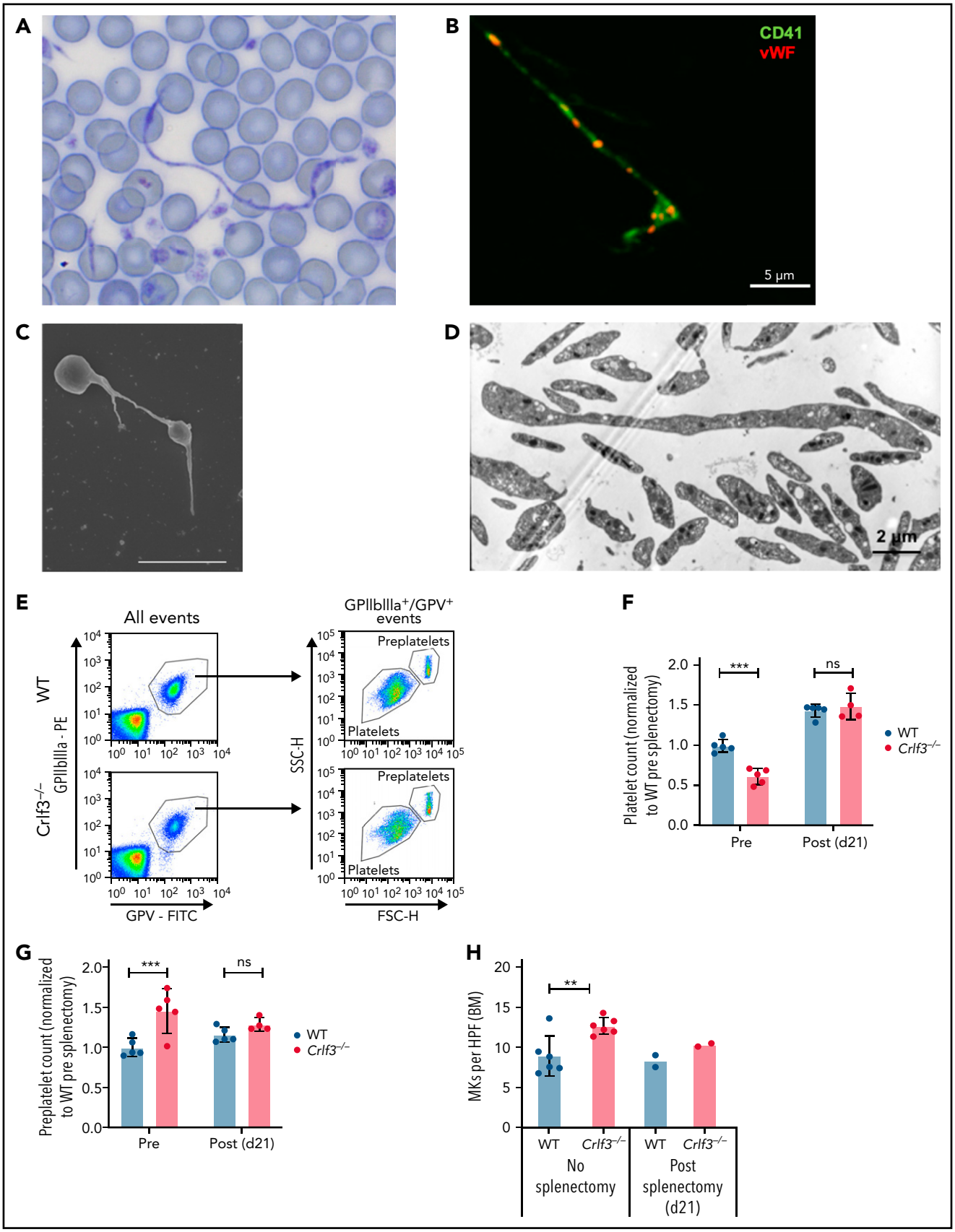

Figure 2. CRLF3 deficiency causes ineffective thrombopoiesis. (A) Romanovsky-stained blood smear from *Crlf3*$^{-/-}$ mouse whole blood taken at 100× magnification under light microscopy. (B) *Crlf3*$^{-/-}$ blood smear stained with CD41 (green) and von Willebrand factor (VWF; red) and imaged by confocal microscopy. (C,D) Washed *Crlf3*$^{-/-}$ platelets fixed and prepared for scanning (C) or transmission electron microscopy (D). Scale bars are 5 µm (B,C) and 2 µm (D). (E-G) Example flow cytometric

supplemental Figure 3D). Thrombus formation of whole blood flowed at arterial shear rates over a collagen-coated surface was equally efficient ($P = .9809$; supplemental Figure 3E). Finally, we determined platelet lifespan by flow cytometry. We found that the gradual decrease in labeled platelets was identical in both control and *Crlf3*$^{-/-}$ animals, suggesting that platelet lifespan is unaffected (Figure 1M).

Crlf3 deficiency leads to ineffective thrombopoiesis

Preplatelets released into the BM sinusoids resemble proplatelet shafts, barbell platelets, or giant platelets.[1,2] Preplatelets were rarely seen on the blood smears of control mice (supplemental Figure 4A) but were easily identified on *Crlf3*$^{-/-}$ samples. Remarkably, some of these were several hundred microns in length, with the classical beads-on-a-string appearance, which has been reported before in culture but not in the peripheral circulation (Figure 2A; supplemental Figure 4A). We confirmed that these structures were preplatelets using immunofluorescence staining for specific platelet cell surface markers (CD41) and proteins contained in platelet α-granules, including von Willebrand factor (Figure 2B), and using scanning (Figure 2C; supplemental Figure 4B) and transmission (Figure 2D; supplemental Figure 4C) electron microscopy. We hypothesized that lack of CRLF3 impairs preplatelet fission and that a proportion of these circulating hyperstable preplatelets are removed from the peripheral circulation (primarily in the spleen) before they have the chance to mature into platelets. This would decrease the number of new platelets produced by each MK (ineffective thrombopoiesis). We hypothesized that splenectomy would allow the preplatelets to circulate longer, allowing them to undergo fission and correct the platelet count. We measured circulating platelet and preplatelet counts by flow cytometry pre- and postsplenectomy by a published method[3] (Figure 2E). Spleen size and weight as well as histology were comparable between *Crlf3*$^{-/-}$ and control animals (supplemental Figure 4E). Control animals showed a slight increase in the platelet count as expected postsplenectomy (Figure 2F). The platelet count in splenectomized *Crlf3*$^{-/-}$ animals also increased postsurgery but crucially reached the same level as that seen in the control animals ($P = .4344$) despite being 38% lower before splenectomy ($P < .0001$). Preplatelets were more abundant in the *Crlf3*$^{-/-}$ animals presplenectomy ($P = .0010$; Figure 2G). Postsplenectomy, circulating preplatelets increased marginally in control animals but decreased in *Crlf3*$^{-/-}$ animals to levels like those seen in the controls ($P = .2524$; Figure 2G). We postulate that splenectomy allows *Crlf3*$^{-/-}$ preplatelets to circulate for long enough to mature into platelets (switching from ineffective to effective thrombopoiesis), thereby improving the number of platelets produced per MK. In keeping with this, postsplenectomy, MK numbers in the BM of *Crlf3*$^{-/-}$ animals reduced toward levels seen in control animals (Figure 2H).

Crlf3$^{-/-}$ MKs contain hyperstable polyglutamylated microtubules

Platelet genesis is driven by microtubule assembly and reorganization. Proplatelet formation and preplatelet release rely on microtubule formation in the proplatelet shaft, whereas preplatelet maturation into mature platelets requires tubulin bundle twisting, followed by disassembly and severing. Tubulin staining in control platelets and a majority of the mature *Crlf3*$^{-/-}$ platelets showed the classical peripheral coil (Figure 3A-D). However, some *Crlf3*$^{-/-}$ platelets had disorganized tubulin, particularly in preplatelets (Figure 3C-D). Most control platelets fully disassembled their microtubule coil upon cooling to 4°C, whereas a significantly larger proportion of *Crlf3*$^{-/-}$ platelets retained at least partially some of the marginal band (41% ± 4% vs 14% ± 1%; $P = .0003$; Figure 3E-I). Microtubule stability is influenced by posttranslational modifications (PTMs), such as tyrosination, acetylation, or glutamylation.[26-28] We saw no difference in the total tubulin content ($P = .1978$), tubulin tyrosination ($P = .7218$), or tubulin acetylation ($P = .1312$) of cultured *Crlf3*$^{-/-}$ MKs, normalized to total tubulin content (Figure 3J; supplemental Figure 5A-C). However, polyglutamylated tubulin content appeared increased in cultured *Crlf3*$^{-/-}$ MKs, although not reaching significance (1.85-fold increase; $P = .0713$; Figure 3J). We therefore probed MK samples with an alternative antibody against polyglutamylated tubulin and showed a similar small increase in polyglutamylated tubulin content (1.66-fold; $P = .0050$; supplemental Figure 5D). Platelet tubulin content and modified tubulins were also analyzed but failed to reveal any significant differences; however, there was a trend toward increased tyrosinated tubulin in platelets (1.47-fold increase; $P = .0639$; Figure 3K; supplemental Figure 5A-C). We postulate that polyglutamylated tubulin was unchanged in platelets, because those would be most likely arising from MKs with the lowest level of glutamylation, allowing for prompt proplatelet maturation. Using immunofluorescence, we showed bundles of glutamylated tubulin leading toward the proplatelet shafts in some *Crlf3*$^{-/-}$ MKs (Figure 3L), but this was not the case in all cells analyzed (supplemental Figure 5E).

CRLF3 interacts with STK38, and its absence leads to increased MOB1 phosphorylation

To gain a mechanistic understanding the role of CRLF3 in tubulin glutamylation, we switched over to a human cellular system. First, we sought to identify the CRLF3 cellular localization and protein partners in relevant cells (ie, platelets and MKs). Human platelet lysates were subfractionated by sucrose gradient centrifugation.[36] Western blot analysis clearly showed enrichment of CRLF3 in the subfractions containing cytoskeletal proteins, particularly α-tubulin (Figure 4A). To refine the localization of CRLF3 and perform pull-down experiments, we used a human iPSC–based system. We inserted a TAP tag[37] at the 3′ end of the endogenous *CRLF3* gene in iPSCs. Tagged and untagged control iPSCs were differentiated into highly pure populations of MKs (Figure 4B) by forward programming.[27] The expression of CRLF3 TAP was confirmed in both tagged iPSCs and their MK

Figure 2 (continued) plots (E) to determine platelet ($GPV^+/GPIIbIIIa^+$ events) (F) and preplatelet ($GPV^+/GPIIbIIIa^+$ events with larger forward scatter [FSC]/side scatter [SSC] than mature platelets) (G) counts from control (WT; blue) and *Crlf3*$^{-/-}$ (red) splenectomized mice (n = 4 *Crlf3*$^{-/-}$ postsplenectomy; n = 5 all other groups). (H) Quantification of MKs in hematoxylin and eosin–stained sections of control (WT; blue) and *Crlf3*$^{-/-}$ (red) tibia of nonsplenectomized animals (left) or 21 postsplenectomy (right; n = 6 non-splenectomized and 2 splenectomized). Data represent means ± standard deviations (except splenectomized mice in panel H, where data represent means). Two-way analysis of variance with correction for multiple comparisons using the Holm-Sidak method (F,G) and unpaired 2-tailed Student *t* test (H). $^{**}P < .01$, $^{***}P < .005$. FITC, fluorescein isothiocyanate; HPF, high-powered field; ns, not significant; PE, phycoerythrin.

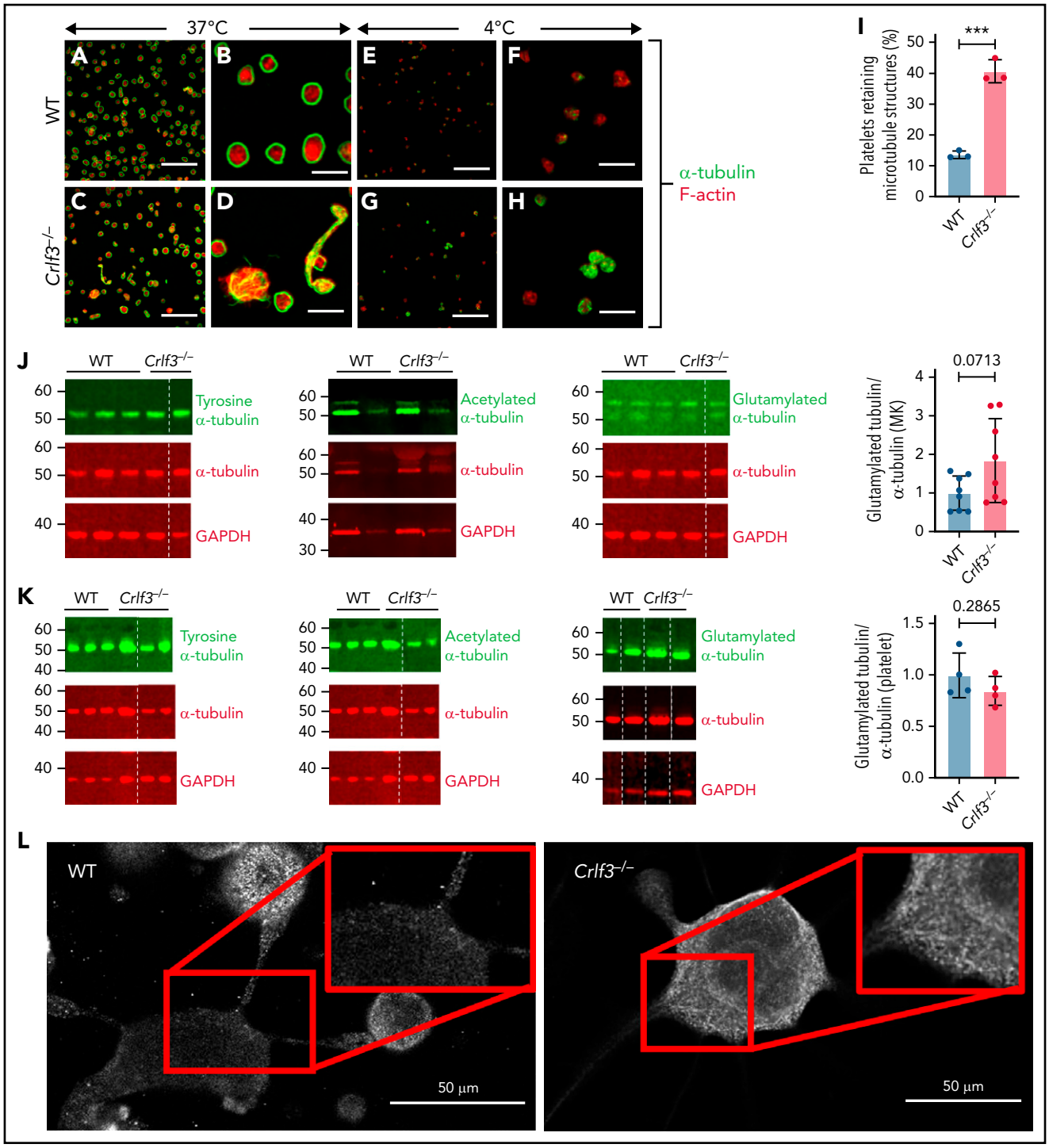

Figure 3. CRLF3 deficiency causes microtubule hyperstability. (A-H) Washed platelets maintained at 37°C (control [WT]) (A,B) (*Crlf3*$^{-/-}$) (C,D) or stored at 4°C for 3 hours (control [WT]) (E,F) (*Crlf3*$^{-/-}$) (G,H) adhered to poly-L-lysine–coated coverslips and stained for α-tubulin (green) and F-actin (red). Scale bars are 20 µm (A,C,E,G) and 5 µm (B,D,F,H). (I) Platelets retaining microtubule structures after incubation at 4°C were determined by manual counting of images for control (WT; blue) and *Crlf3*$^{-/-}$ (red) mice (n = 3). (J-K) Representative western blots of in vitro cultured MK (J) or platelet (K) lysates against tyrosine α-tubulin, α-tubulin, and glyceraldehyde-3-phosphate dehydrogenase (GAPDH; left); acetylated α-tubulin, α-tubulin, and GAPDH (middle); or glutamylated α-tubulin (AG-20B-0020_upper band), α-tubulin, and GAPDH (right) for control (WT; blue) and *Crlf3*$^{-/-}$ (red) samples. The quantification of glutamylated α-tubulin/total tubulin in in vitro cultured MKs (bar graphs on right) was carried out on 8 control and 8 *Crlf3*$^{-/-}$ samples with 2 technical replicates. Where α-tubulin and GAPDH panels are the same for multiple tubulin modifications, membranes were stripped and reprobed between antibodies against specific tubulin modifications before finally being stripped and reprobed for α-tubulin and GAPDH. (L) In vitro cultured MKs were seeded onto fibrinogen-coated coverslips and incubated at 37°C for 5 hours to induce proplatelet formation. Samples were fixed, stained for polyglutamylated α-tubulin (AG-20B-0020), and imaged by fluorescence microscopy. Images are representative for *Crlf3*$^{-/-}$ and control (WT) proplatelet-forming MKs. Scale bars are 50 µm. Data represent means ± standard deviations. Unpaired 2-tailed Student (I,K) or Welch (J) *t* test. ***$P < .005$.

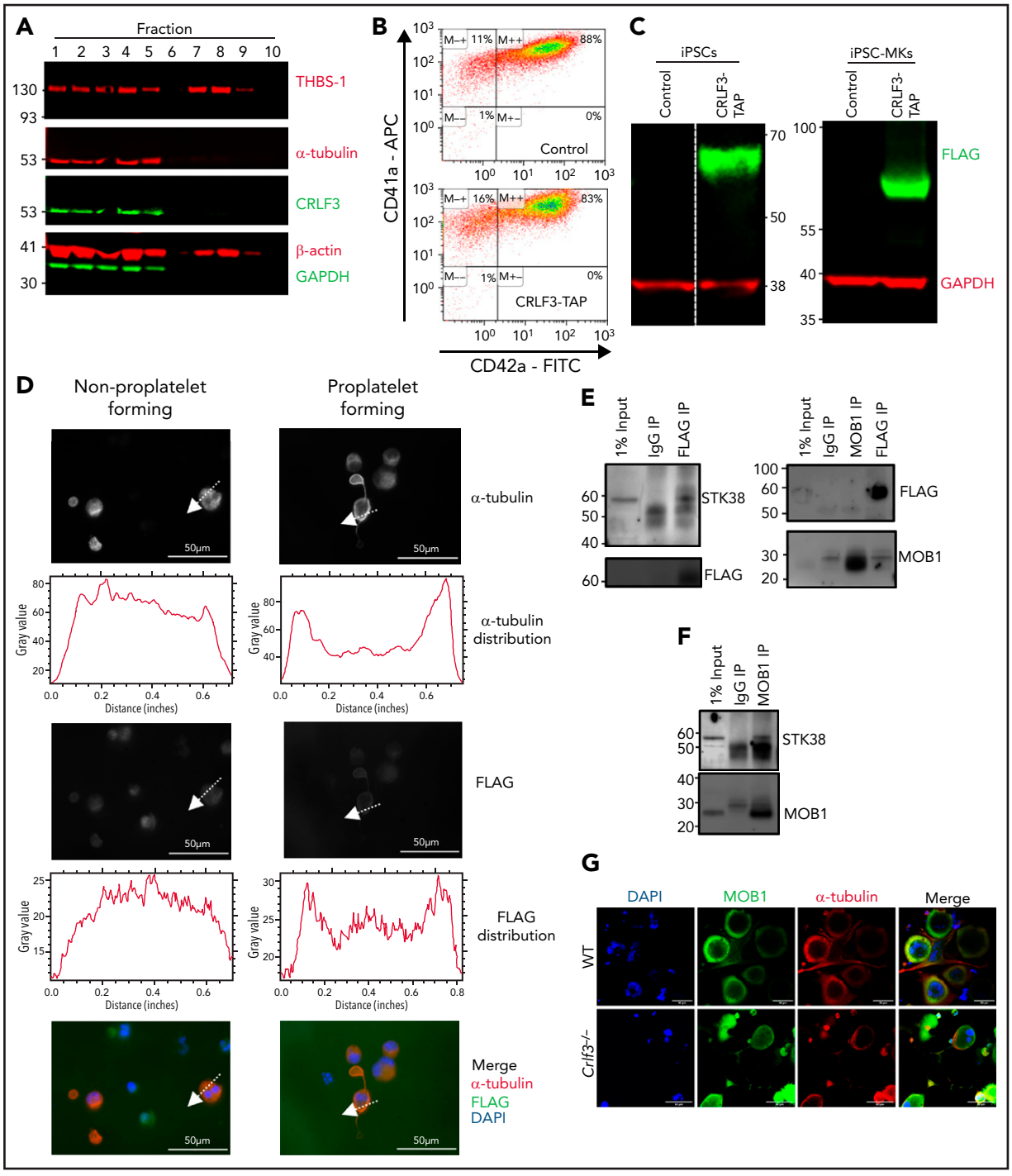

Figure 4. CRLF3 interacts with the Hippo pathway. (A) Western blot of sucrose gradient centrifugation fractionated human platelets probed with antibodies against α-tubulin, β-actin, thrombospondin (THBS-1), glyceraldehyde-3-phosphate dehydrogenase (GAPDH), and CRLF3. Fractions 1 to 5 represent cytoskeletal proteins (enriched for α-tubulin and β-actin), whereas fractions 7 and 8 represent granular proteins (enriched for THBS-1). (B) Representative flow cytometric plots of CRLF3 TAP-tagged and control forward programmed iPSC MKs stained with CD41a and CD42a. (C) Western blot of CRLF3 TAP-tagged and control iPSCs and iPSC MKs probed with antibodies against FLAG (green) and GAPDH (red). (D) CRLF3 TAP-tagged iPSC MKs were seeded onto fibrinogen-coated coverslips and incubated at 37°C for 24 hours to induce proplatelet formation. Samples were fixed, stained with α-tubulin (red), FLAG (green), and DAPI (blue), and imaged by fluorescence microscopy. Subcellular distribution of α-tubulin and FLAG staining in round and proplatelet-forming CRLF3 TAP iPSC MKs was determined across a section of the MKs along the indicated arrow using ImageJ. Scale bars are 50 μm. (E-F) CRLF3 TAP (E) and control (F) iPSC MKs were lysed and immunoprecipitated (IP) with antibodies against FLAG, MOB1, and immunoglobulin G (IgG). Precipitated lysates were then probed for STK38, MOB1, and FLAG by western blot. (G) In vitro cultured MKs were seeded onto fibrinogen-coated coverslips and incubated at 37°C for 5 hours to induce proplatelet formation. Samples were fixed, stained for MOB1 (green), α-tubulin (red), and DAPI (blue), and imaged by fluorescence microscopy. Images are representative for *Crlf3*$^{-/-}$ and control (WT) proplatelet-forming MKs. (H) Western blot of in vitro cultured MKs probed with antibodies against pMOB1, MOB1, and GAPDH (left panel; n = 8 MOB1/GAPDH and 4 pMOB1/GAPDH) and pSTK38, STK38 and GAPDH (right panel; n = 3 STK38/GAPDH, 3 *Crlf3*$^{-/-}$, and 4 WT pSTK38/GAPDH). (I) Three-dimensional structure of CRLF3 (residue 174 to end) solved by experimental phasing. Domains are labeled. Molecular graphics prepared using PyMOL. Data represent means ± standard deviations. Unpaired 2-tailed Student *t* test. **P* < .05. FITC, fluorescein isothiocyanate; FN3, fibronectin type 3.

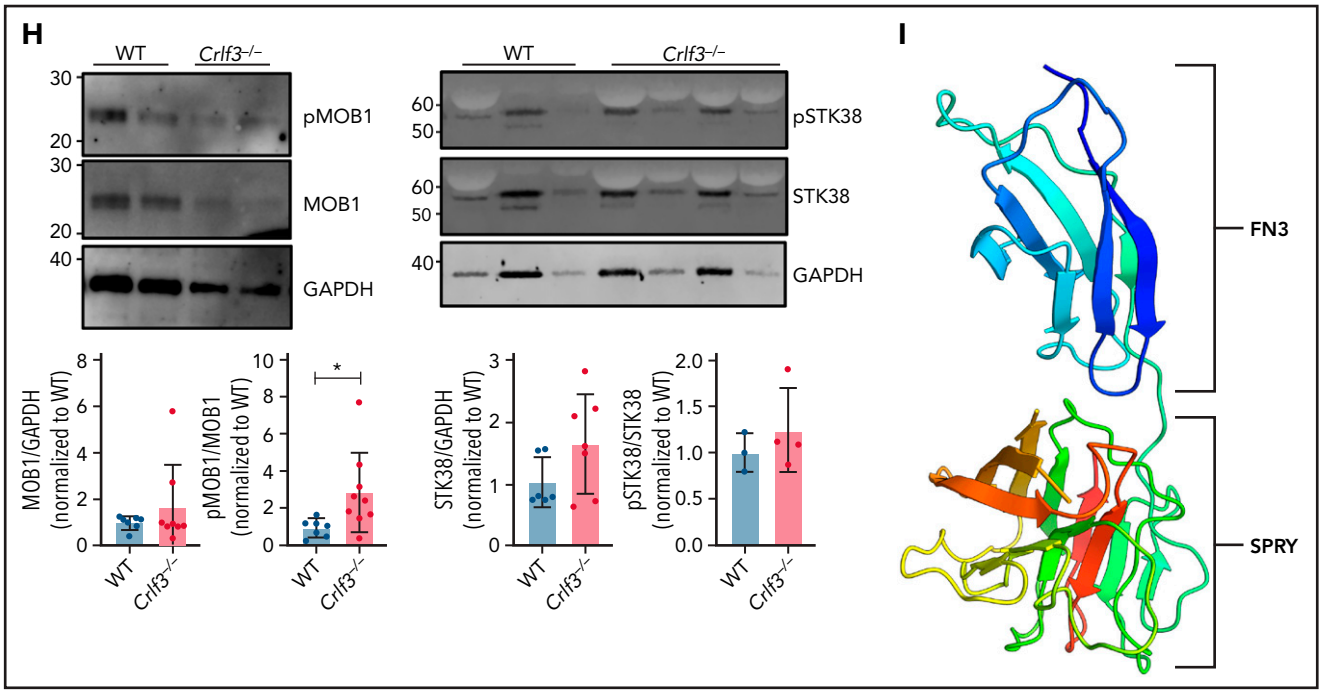

Figure 4. (continued)

progeny (iPSC MKs; Figure 4C). In non–proplatelet-forming iPSC MKs, CRLF3 TAP showed a diffuse mainly cytoplasmic pattern. By contrast, in proplatelet-forming iPSC MKs, CRLF3 TAP appears to redistribute to the plasma membrane (Figure 4D). We went on to perform mass spectrometry on anti-FLAG immunoprecipitation samples from CRLF3 TAP and control iPSC MKs, and several candidate interacting proteins were identified (supplemental Table 2). One candidate interactor was STK38, a member of a group of NDR kinases known to interact with MOB1.[38] MOB1 is a key member of the Hippo pathway[39] and a protein that has been shown to influence tubulin stability through PTMs.[40] MOB1 has previously been shown to interact with CRLF3 in HEK cells treated with okadaic acid.[41,42] We performed anti-FLAG immunoprecipitation followed by western blotting on okadaic acid–treated CRLF3-tagged iPSC MKs and confirmed the interaction between CRLF3 and STK38 (Figure 4E). We could not show evidence of an interaction between CRLF3 and MOB1 in either the forward or reverse pull downs (Figure 4E); however, in anti-MOB1 immunoprecipitated control iPSC MKs, we confirmed the interaction between MOB1 and STK38 (Figure 4F). We did not see a difference in MOB1 localization (Figure 4G) or total quantity of MOB1 (P = .3337; Figure 4H) in *Crlf3*$^{-/-}$ MKs. However, we saw increased phosphorylation of MOB1 (>2.5-fold; P = .0286; Figure 4H; supplemental Figure 6). Because we had established an interaction between CRLF3 and STK38 in MKs, we looked at the influence of CRLF3 on STK38 protein. We saw a small (~1.5-fold) nonsignificant increase in total quantity of STK38 (P = .1112; Figure 4H) in *Crlf3*$^{-/-}$ MKs, but STK38 phosphorylation was unchanged (P = .4398).

Finally, we sought to determine the crystal structure of CRLF3. We were successful only in expressing the C-terminal portion of CRLF3 (amino acids 174-442) at sufficient levels for crystallography. Crystals were successfully obtained using the sitting drop vapor diffusion method. Native data were collected to a resolution of 1.61 Å, and the structure was solved by Hg single-wavelength anomalous diffraction phasing. This revealed a 3-dimensional structure containing 2 known protein-binding domains, a fibronectin type 3 domain (residues 179-273) and a SPRY domain (residues 274-442; Figure 4I). Crystallographic statistics can be found in supplemental Table 3. The native structure, refined to R_{work} = 0.177 and R_{free} = 0.201, has been deposited at the Worldwide Protein Data Bank with ID 6RPX.

CRLF3 in human thrombopoiesis

We used a genetic approach to look for evidence that CRLF3 and its partners play a role in human thrombopoiesis. Using the imputed genotype data from 403 112 European ancestry participants in UK Biobank, we performed univariable association analyses between 29 hematological traits and genetic variants in the loci containing CRLF3, MOB1A, and STK38. Our analyses identified significant ($-\log_{10} P > 8.08$) associations with platelet distribution width in the CRLF3 locus (Figure 5A, left panel), of which the variant with the strongest evidence for association (rs6505211; purple diamond) was in the gene body. This variant was in high linkage disequilibrium ($r^2 > 0.8$) with the variant exhibiting the strongest evidence for association with platelet distribution width but also with lymphocyte percentage of total white blood cells. We also identified associations with variants in STK38, which were significantly associated with mean platelet volume (Figure 5A, right panel) and identified a variant in MOB1A significantly associated with platelet count (supplemental Table 4). The latter variant is not associated with other hematological traits. These data therefore suggest a role for all 3 genes in thrombopoiesis, without necessarily implying that there is a mechanistic link among them.

Among a collection of 59 464 individuals comprising probands affected with rare disorders for whom human platelet ontology

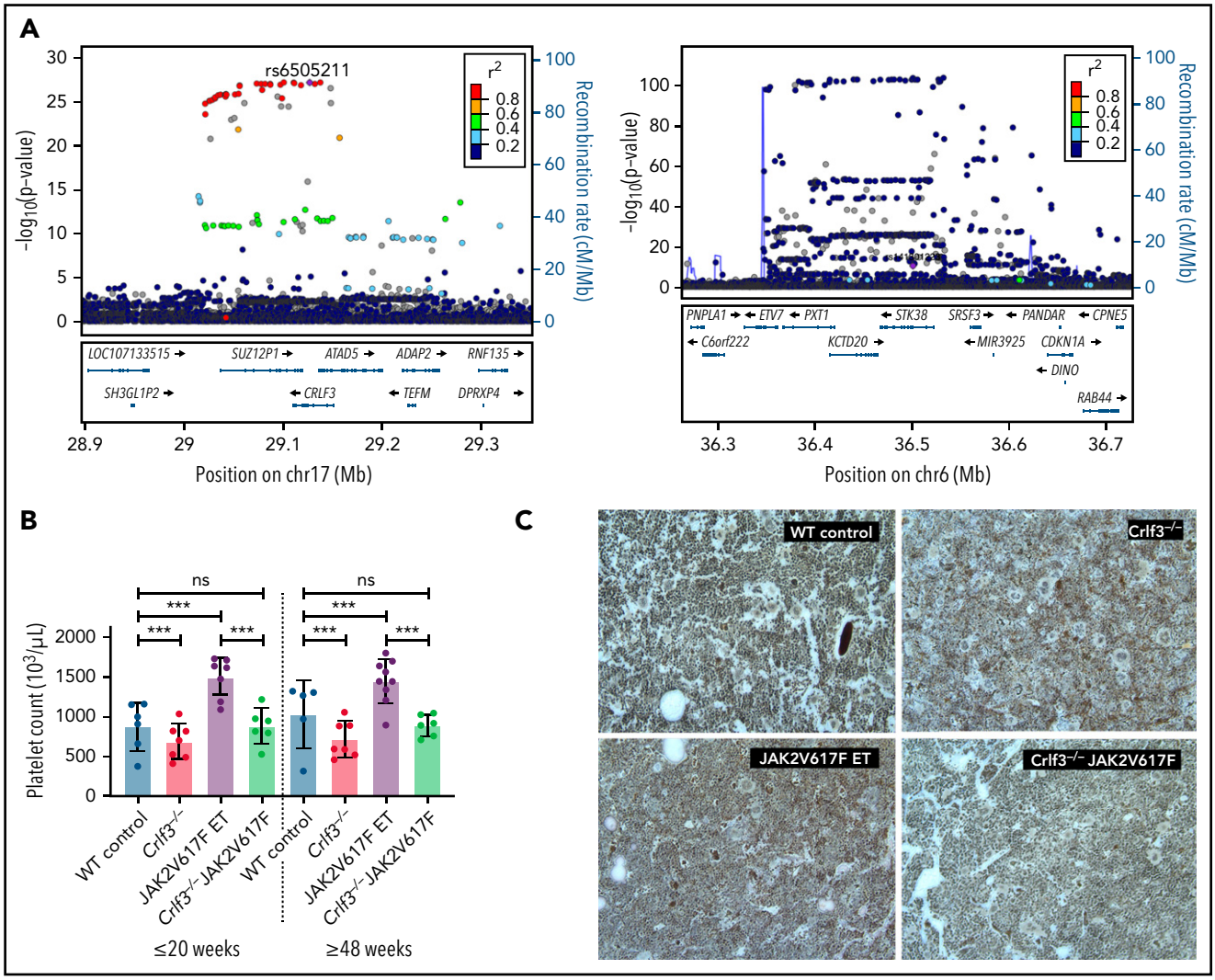

Figure 5. CRLF3 regulates platelet traits in humans and is a therapeutic target for ET. (A) Locuszoom of CRLF3 (left) and STK38 (right) showing variants associated with platelet distribution width (PDW) and mean platelet volume, respectively. The conditionally independent variant is indicated by a purple diamond; linkage disequilibrium (LD) values (r^2) with this variant are indicated by dot colors according to the legend. The CRLF3 locuszoom plot shows the conditionally independent variant (rs6505211: −log10P, 27.1; MAF, 17.6%) is in high LD with a number of variants, which are significantly associated with PDW. In the case of STK38, the locuszoom plot indicates that the conditionally independent variant (rs141301223: −log10P, 10.4; MAF, 0.041%) is not in high LD with nearby variants (common for rare variant associations). (B) Platelet counts from young (≤20 weeks) and old (≥48 weeks) female WT control (blue; n = 6 young and 5 old), *Crlf3*$^{-/-}$ (red; n = 7 young and 7 old), JAK2 V617F ET (purple; n = 7 young and 9 old), and *Crlf3*$^{-/-}$ JAK2 V617F (green; n = 6 young and 6 old) mice. (C) Fixed tibia sections stained with Gömöri reticulin silver stain and imaged by light microscopy at 20× magnification. Images are representative of 3 mice per genotype. Data represent means ± standard deviations. Two-way analysis of variance with correction for multiple comparisons using the Holm-Sidak method. ***$P < .005$. ns, not significant.

terms were available and their first-degree relatives, we identified 27 who were heterozygous for severe impact variants in *CRLF3*. None had human platelet ontology terms suggesting a hematological phenotype (supplemental Table 5). No homozygous individuals for severe impact variants were identified in this cohort. Five individuals (including 2 siblings) were identified who were homozygous for missense variants, but again, none had a hematological phenotype. The severe variants were shown to be low frequency in gnomAD.[34,43] The missense variants were inputted into the crystal structure described. Ala279Val and Asn410Asp have MAFs of 2.4×10^{-5} and 4.7×10^{-4} in gnomAD, respectively, but are minor changes on the surface of the protein. Leu389Pro has an MAF of 15% and together with the last variant, Thr392Ile, is part of a disordered loop (amino acids 387-398), again on the surface of the protein.

CRLF3 is a potential therapeutic target for ET

We postulated that the specific effect of CRLF3 deficiency on platelet count would make CRLF3 a potential therapeutic target in ET. As a proof of principle, we crossbred *Crlf3*$^{-/-}$ mice with a previously published inducible knock-in mouse model of ET driven by the JAK2 V617F mutation.[44] The breeding strategy described in supplemental Figure 7 generated 4 groups of animals: WT control, *Crlf3*$^{-/-}$, JAK2 V617F ET, and *Crlf3*$^{-/-}$ JAK2 V617F mice. We assessed the platelet counts in these 4 groups of mice at both young (≤20 weeks) and old (≥48 weeks) ages and showed that ablation of *Crlf3* in JAK2 V627F ET mice normalized the platelet count to the levels seen in control mice (Figure 5B). Crucially, we showed that all other blood counts were unaffected (supplemental Table 6). Platelet function analysis in all 4 groups of mice showed no differences. No additional

clinical findings were made in the *Crlf3*$^{-/-}$ JAK2V627F mice, including no evidence of BM fibrosis (Figure 5C) or changes in spleen size/weight (data not shown).

Discussion

Thrombopoiesis is classically described as a 2-stage process comprising first MK differentiation and maturation from HSCs followed by the actual process of platelet release. Proplatelet formation, which has been observed in vivo,[1,2] is the broadly accepted mechanism by which MKs release platelets, although some authors have argued that MK fragmentation[45] or membrane budding[46] may constitute an alternative mechanism. Proplatelet fragments detach from MKs, forming long beads-on-a-string structures (preplatelets) that become mature discoid platelets.[3] In this report, we show that preplatelet fission is critical for regulating platelet production and is the third and final stage of platelet production. We show that mice deficient in CRLF3 have reduced platelet counts resulting from ineffective thrombopoiesis, whereby slowed maturation of circulating preplatelets leads to their removal by the spleen, reducing the number of circulating platelets. These data clearly suggest the central role of proplatelet formation and subsequent preplatelet fission in platelet biogenesis as opposed to MK fragmentation or blebbing.

It has long been known that proplatelet formation is a process in which cytoskeletal proteins play a key role. Our data suggest that CRLF3 deficiency may exert its effect on preplatelet maturation through increasing tubulin stability. We show small changes in tubulin polyglutamylation in the primary mouse MKs, which may in part explain these observations. This would need to be confirmed in MKs derived from cell lines, rather than primary MKs, to allow for detailed protein and PTM studies to be carried out. We should note that it has been shown using cell line models that tubulin polyglutamylation promotes proplatelet-like extensions in CHO cells[47] and affects the localization of motor protein in MKs.[48] In keeping with this, we observed an increased rate of proplatelet formation in *Crlf3*$^{-/-}$ MKs. The tubulin C-terminal tail is subjected to diverse PTMs, which vary among cell type and intracellular localization.[49] This allows fine spatial and temporal control of microtubule function by modifying the binding of microtubule-associated proteins (including microtubule-severing enzymes). Although the key enzymes involved in controlling tubulin glutamylation and severing are expressed equally between *Crlf3*$^{-/-}$ and control MKs (supplemental Table 7), we postulate that the increase in tubulin glutamylation observed in the *Crlf3*$^{-/-}$ MKs is such that it may subsequently affect tubulin severing in the *Crlf3*$^{-/-}$ preplatelets, thereby preventing their maturation. This hypothesis deserves further study, potentially using genetically modified MKs derived from cell lines enabling fine tuning of tubulin polyglutamylation to examine proplatelet formation and maturation dynamics.

Direct interaction between CRLF3 and MOB1 has been previously reported.[41,42] MOB1 acts as a coactivator of NDR kinases, including STK38.[38] MOB1 phosphorylation increases its binding to and activation of STK38[39] and localizes the complex to the plasma membrane, especially at sites of pseudopodia/cytoplasmic extensions.[50] MOB1 is known to affect tubulin stability through regulating acetylation and thereby cytokinesis.[40] In this study, we confirmed that, in MKs, STK38 is associated with both MOB1 and CRLF3, but we did not show a direct interaction between CRLF3 and MOB1. However, MOB1 phosphorylation was increased in *Crlf3*$^{-/-}$ MKs, and we also showed that CRLF3 relocates to the membrane, but only in proplatelet-forming MKs. Taken together, these data strongly support the need for additional studies in MKs to provide definitive proof that MOB1 influences PTMs of tubulin in MKs and thereby influences proplatelet formation and maturation dynamics and ultimately circulating platelet numbers.

Most patients with ET are administered nonspecific cytoreductive therapies to lower their platelet count. Hydroxyurea, the most commonly prescribed agent, causes anemia, leukopenia, or skin ulcers[51,52] in up to 20% of patients, and concerns about an associated leukemic risk remain.[53,54] Anagrelide, the second most commonly prescribed agent, is associated with a threefold increased risk of myelofibrosis compared with hydroxyurea.[55] Identification of a novel biological pathway that, when targeted, could specifically reduce platelet count is promising for the treatment of ET. Targeting CRLF3 may allow specific reductions in platelet count by acting at the level of preplatelet maturation, as evidenced with our *Crlf3*$^{-/-}$ JAK2 V617F ET murine model. These mice showed sustained and isolated normalization of their platelet count without increased BM fibrosis or leukemic transformation. An increased understanding of the role of CRLF3 in other cell types, its structure, and its structural relationship with partner proteins, such as STK38 and MOB1, as well as a definition of how CRLF3 interacts with tubulin after translation modifications, could potentially generate drugs that would complement (or supersede) the current nonspecific cytoreductive agents. Additional studies of the role of CRLF3 should also focus on the human system to confirm the findings of the murine studies presented here.

Acknowledgments

The authors acknowledge Tina Hamilton and Dean Pask for their expertise in and time with animal ethics and assistance with animal experiments. The authors also thank Jeremy Skepper for processing samples for scanning electron microscopy.

This work was supported by the British Heart Foundation (PhD Studentship FS/14/40/30921). This research was funded in part by the Wellcome Trust (203151/Z/16/Z) and the UKRI Medical Research Council (MC_PC_17230). For the purpose of open access, the authors have applied a CC BY public copyright license to any Author Accepted Manuscript version arising from this submission. M.B. is supported by an Emmy Noether grant of the Deutsche Forschungsgemeinschaft (BE5084/3-1).

Authorship

Contribution: C.B. conceptualized the idea, designed and performed experiments, analyzed and interpreted data, and wrote manuscript; J.A.G. and M.L. conceptualized the idea, designed and performed experiments, analyzed and interpreted data, and revised the manuscript; S.S., A.K.W., Y.Y., R.W.M., J.B.-B., A.B., A.M., J.W., C.J.P., and P.A. designed and performed experiments and analyzed and interpreted data; L.M., T.M., A.L.E., S.M., G.J.H., and K.S.-P. designed experiments and interpreted data; D.J.A. conceptualized the idea and designed experiments; A.L.C. interpreted data and revised the manuscript; M.B. designed and performed experiments, analyzed and interpreted data, and revised the manuscript; W.N.E. performed experiments, interpreted data, and revised the manuscript; B.N. interpreted data and revised the manuscript; R.J.R. designed experiments, interpreted data, and revised the manuscript; and C.G. conceptualized the idea, designed experiments, interpreted data, and wrote the manuscript.

Conflict-of-interest disclosure: P.A. is a full-time employee of Regeneron pharmaceuticals and currently holds options and stock of the company. The remaining authors declare no competing financial interests.

ORCID profiles: C.B., 0000-0002-9796-9381; M.L., 0000-0001-9386-5633; A.K.W., 0000-0002-9726-5560; Y.Y., 0000-0001-6934-9874; J.B.-B., 0000-0002-3287-2925; L.M., 0000-0003-4905-0669; J.W., 0000-0003-1060-1865; C.J.P., 0000-0003-4006-7261; P.A., 0000-0001-9210-4760; T.M., 0000-0003-1090-6685; S.M., 0000-0003-4904-1324; K.S.-P., 0000-0002-0633-3696; D.J.A., 0000-0001-9490-0306; A.L.C., 0000-0003-0057-6686; M.B., 0000-0002-2381-116X; W.N.E., 0000-0002-1028-9376; B.N., 0000-0003-1454-7413; R.J.R., 0000-0001-8273-0047; C.G., 0000-0002-9251-0934.

Correspondence: Cavan Bennett, Cambridge Blood Centre, Long Road, Cambridge, CB20PT United Kingdom; e-mail: cavanbennett89@gmail.com; and Cedric Ghevaert, Wellcome-MRC Cambridge Stem Cell Institute, Jeffrey Cheah Biomedical Centre, Cambridge Biomedical Campus, University of Cambridge, Puddicombe Way, Cambridge CB2 0AW, United Kingdom; e-mail: cg348@cam.ac.uk.

Footnotes

Submitted 28 June 2021; accepted 23 November 2021; prepublished online on *Blood* First Edition 20 January 2022. DOI 10.1182/blood.2021013113.

CRLF3 structures have been deposited in the Worldwide Protein Data Bank under accession numbers 6RPX, 6RPY, and 6RPZ. The mass spectrometry proteomics data have been deposited to the ProteomeXchange Consortium via the PRIDE partner repository with the dataset identifier PXD017026. For original data, please contact cg384@cam.ac.uk.

The online version of this article contains a data supplement.

There is a *Blood* Commentary on this article in this issue.

The publication costs of this article were defrayed in part by page charge payment. Therefore, and solely to indicate this fact, this article is hereby marked "advertisement" in accordance with 18 USC section 1734.

REFERENCES

1. Zhang L, Orban M, Lorenz M, et al. A novel role of sphingosine 1-phosphate receptor S1pr1 in mouse thrombopoiesis. *J Exp Med.* 2012;209(12):2165-2181.
2. Junt T, Schulze H, Chen Z, et al. Dynamic visualization of thrombopoiesis within bone marrow. *Science.* 2007;317(5845):1767-1770.
3. Thon JN, Montalvo A, Patel-Hett S, et al. Cytoskeletal mechanics of proplatelet maturation and platelet release. *J Cell Biol.* 2010;191(4):861-874.
4. Kunishima S, Nishimura S, Suzuki H, Imaizumi M, Saito H. TUBB1 mutation disrupting microtubule assembly impairs proplatelet formation and results in congenital macrothrombocytopenia. *Eur J Haematol.* 2014;92(4):276-282.
5. Pecci A, Klersy C, Gresele P, et al. MYH9-related disease: a novel prognostic model to predict the clinical evolution of the disease based on genotype-phenotype correlations. *Hum Mutat.* 2014;35(2):236-247.
6. Nurden P, Debili N, Coupry I, et al. Thrombocytopenia resulting from mutations in filamin A can be expressed as an isolated syndrome. *Blood.* 2011;118(22):5928-5937.
7. Kunishima S, Okuno Y, Yoshida K, et al. ACTN1 mutations cause congenital macrothrombocytopenia. *Am J Hum Genet.* 2013;92(3):431-438.
8. Pleines I, Woods J, Chappaz S, et al. Mutations in tropomyosin 4 underlie a rare form of human macrothrombocytopenia. *J Clin Invest.* 2017;127(3):814-829.
9. Stritt S, Nurden P, Turro E, et al; BRIDGE-BPD Consortium. A gain-of-function variant in DIAPH1 causes dominant macrothrombocytopenia and hearing loss. *Blood.* 2016;127(23):2903-2914.
10. Baxter EJ, Scott LM, Campbell PJ, et al; Cancer Genome Project. Acquired mutation of the tyrosine kinase JAK2 in human myeloproliferative disorders. *Lancet.* 2005;365(9464):1054-1061.
11. Levine RL, Wadleigh M, Cools J, et al. Activating mutation in the tyrosine kinase JAK2 in polycythemia vera, essential thrombocythemia, and myeloid metaplasia with myelofibrosis. *Cancer Cell.* 2005;7(4):387-397.
12. Kralovics R, Passamonti F, Buser AS, et al. A gain-of-function mutation of JAK2 in myeloproliferative disorders. *N Engl J Med.* 2005;352(17):1779-1790.
13. James C, Ugo V, Le Couédic JP, et al. A unique clonal JAK2 mutation leading to constitutive signalling causes polycythaemia vera. *Nature.* 2005;434(7037):1144-1148.
14. Klampfl T, Gisslinger H, Harutyunyan AS, et al. Somatic mutations of calreticulin in myeloproliferative neoplasms. *N Engl J Med.* 2013;369(25):2379-2390.
15. Nangalia J, Massie CE, Baxter EJ, et al. Somatic CALR mutations in myeloproliferative neoplasms with nonmutated JAK2. *N Engl J Med.* 2013;369(25):2391-2405.
16. Pardanani AD, Levine RL, Lasho T, et al. MPL515 mutations in myeloproliferative and other myeloid disorders: a study of 1182 patients. *Blood.* 2006;108(10):3472-3476.
17. Pikman Y, Lee BH, Mercher T, et al. MPLW515L is a novel somatic activating mutation in myelofibrosis with myeloid metaplasia. *PLoS Med.* 2006;3(7):e270.
18. Dombi P, Illés Á, Demeter J, et al. Anagrelide reduces thrombotic risk in essential thrombocythaemia vs. hydroxyurea plus aspirin. *Eur J Haematol.* 2017;98(2):106-111.
19. Yang F, Xu YP, Li J, et al. Cloning and characterization of a novel intracellular protein p48.2 that negatively regulates cell cycle progression. *Int J Biochem Cell Biol.* 2009;41(11):2240-2250.
20. White JK, Gerdin AK, Karp NA, et al; Sanger Institute Mouse Genetics Project. Genome-wide generation and systematic phenotyping of knockout mice reveals new roles for many genes. *Cell.* 2013;154(2):452-464.
21. Ryder E, Gleeson D, Sethi D, et al; Sanger Mouse Genetics Project. Molecular characterization of mutant mouse strains generated from the EUCOMM/KOMP-CSD ES cell resource. *Mamm Genome.* 2013;24(7-8):286-294.
22. Skarnes WC, Rosen B, West AP, et al. A conditional knockout resource for the genome-wide study of mouse gene function. *Nature.* 2011;474(7351):337-342.
23. Hobbs CM, Manning H, Bennett C, et al. JAK2V617F leads to intrinsic changes in platelet formation and reactivity in a knock-in mouse model of essential thrombocythemia. *Blood.* 2013;122(23):3787-3797.
24. McCarty OJ, Zhao Y, Andrew N, et al. Evaluation of the role of platelet integrins in fibronectin-dependent spreading and adhesion. *J Thromb Haemost.* 2004;2(10):1823-1833.
25. Stritt S, Beck S, Becker IC, et al. Twinfilin 2a regulates platelet reactivity and turnover in mice. *Blood.* 2017;130(15):1746-1756.
26. Li J, Kent DG, Godfrey AL, et al. JAK2V617F homozygosity drives a phenotypic switch in myeloproliferative neoplasms, but is insufficient to sustain disease. *Blood.* 2014;123(20):3139-3151.
27. Moreau T, Evans AL, Vasquez L, et al. Large-scale production of megakaryocytes from human pluripotent stem cells by chemically defined forward programming [published correction appears in *Nat Commun.* 2017;8:15076]. *Nat Commun.* 2016;7:11208.
28. Bender M, Stritt S, Nurden P, et al. Megakaryocyte-specific Profilin1-deficiency alters microtubule stability and causes a Wiskott-Aldrich syndrome-like platelet defect [published correction appears in *Nat Commun.* 2015;6:6507]. *Nat Commun.* 2014;5:4746.
29. Stritt S, Nurden P, Favier R, et al. Defects in TRPM7 channel function deregulate thrombopoiesis through altered cellular Mg(2+) homeostasis and cytoskeletal architecture. *Nat Commun.* 2016;7:11097.
30. Mazharian A, Thomas SG, Dhanjal TS, Buckley CD, Watson SP. Critical

role of Src-Syk-PLCgamma2 signaling in megakaryocyte migration and thrombopoiesis. *Blood*. 2010;116(5):793-800.

31. Terwilliger TC, Adams PD, Read RJ, et al. Decision-making in structure solution using Bayesian estimates of map quality: the PHENIX AutoSol wizard. *Acta Crystallogr D Biol Crystallogr*. 2009;65(Pt 6):582-601.

32. Adams PD, Afonine PV, Bunkóczi G, et al. PHENIX: a comprehensive Python-based system for macromolecular structure solution. *Acta Crystallogr D Biol Crystallogr*. 2010;66(Pt 2):213-221.

33. Emsley P, Lohkamp B, Scott WG, Cowtan K. Features and development of Coot. *Acta Crystallogr D Biol Crystallogr*. 2010;66(Pt 4):486-501.

34. Karczewski KJ, Francioli LC, Tiao G, et al. Variation across 141,456 human exomes and genomes reveals the spectrum of loss-of-function intolerance across human protein-coding genes. *bioRxiv*. Preprint posted online 13 August 2019.

35. Turro E, Astle WJ, Megy K, et al; NIHR BioResource for the 100,000 Genomes Project. Whole-genome sequencing of patients with rare diseases in a national health system. *Nature*. 2020;583(7814):96-102.

36. Mayer L, Jasztal M, Pardo M, et al. Nbeal2 interacts with Dock7, Sec16a, and Vac14. *Blood*. 2018;131(9):1000-1011.

37. Pardo M, Lang B, Yu L, et al. An expanded Oct4 interaction network: implications for stem cell biology, development, and disease. *Cell Stem Cell*. 2010;6(4):382-395.

38. Bichsel SJ, Tamaskovic R, Stegert MR, Hemmings BA. Mechanism of activation of NDR (nuclear Dbf2-related) protein kinase by the hMOB1 protein. *J Biol Chem*. 2004;279(34):35228-35235.

39. Praskova M, Xia F, Avruch J. MOBKL1A/MOBKL1B phosphorylation by MST1 and MST2 inhibits cell proliferation. *Curr Biol*. 2008;18(5):311-321.

40. Florindo C, Perdigão J, Fesquet D, Schiebel E, Pines J, Tavares AA. Human Mob1 proteins are required for cytokinesis by controlling microtubule stability. *J Cell Sci*. 2012;125(Pt 13):3085-3090.

41. Couzens AL, Knight JD, Kean MJ, et al. Protein interaction network of the mammalian Hippo pathway reveals mechanisms of kinase-phosphatase interactions. *Sci Signal*. 2013;6(302):rs15.

42. Xiong S, Couzens AL, Kean MJ, et al. Regulation of protein interactions by *M*ps *O*ne *B*inder (MOB1) phosphorylation. *Mol Cell Proteomics*. 2017;16(6):1111-1125.

43. Lek M, Karczewski KJ, Minikel EV, et al; Exome Aggregation Consortium. Analysis of protein-coding genetic variation in 60,706 humans. *Nature*. 2016;536(7616):285-291.

44. Li J, Spensberger D, Ahn JS, et al. JAK2 V617F impairs hematopoietic stem cell function in a conditional knock-in mouse model of JAK2 V617F-positive essential thrombocythemia. *Blood*. 2010;116(9):1528-1538.

45. Nishimura S, Nagasaki M, Kunishima S, et al. IL-1α induces thrombopoiesis through megakaryocyte rupture in response to acute platelet needs. *J Cell Biol*. 2015;209(3):453-466.

46. Potts KS, Farley A, Dawson CA, et al. Membrane budding is a major mechanism of in vivo platelet biogenesis. *J Exp Med*. 2020;217(9):e20191206.

47. van Dijk J, Bompard G, Cau J, et al. Microtubule polyglutamylation and acetylation drive microtubule dynamics critical for platelet formation. *BMC Biol*. 2018;16(1):116.

48. Khan AO, Slater A, Maclachlan A, et al. Post-translational polymodification of β1-tubulin regulates motor protein localisation in platelet production and function. *Haematologica*. 2022;107(1):243-259.

49. Garnham CP, Roll-Mecak A. The chemical complexity of cellular microtubules: tubulin post-translational modification enzymes and their roles in tuning microtubule functions. *Cytoskeleton (Hoboken)*. 2012;69(7):442-463.

50. Hergovich A, Stegert MR, Schmitz D, Hemmings BA. NDR kinases regulate essential cell processes from yeast to humans. *Nat Rev Mol Cell Biol*. 2006;7(4):253-264.

51. Barosi G, Besses C, Birgegard G, et al. A unified definition of clinical resistance/intolerance to hydroxyurea in essential thrombocythemia: results of a consensus process by an international working group [published correction appears in *Leukemia*. 2007;21(5):1135]. *Leukemia*. 2007;21(2):277-280.

52. Alvarez-Larrán A, Pereira A, Guglielmelli P, et al. Antiplatelet therapy versus observation in low-risk essential thrombocythemia with a CALR mutation. *Haematologica*. 2016;101(8):926-931.

53. Birgegård G, Folkvaljon F, Garmo H, et al. Leukemic transformation and second cancers in 3649 patients with high-risk essential thrombocythemia in the EXELS study. *Leuk Res*. 2018;74:105-109.

54. Birgegård G, Besses C, Griesshammer M, et al. Treatment of essential thrombocythemia in Europe: a prospective long-term observational study of 3649 high-risk patients in the Evaluation of Anagrelide Efficacy and Long-term Safety study. *Haematologica*. 2018;103(1):51-60.

55. Tefferi A, Szuber N, Vallapureddy RR, et al. Decreased survival and increased rate of fibrotic progression in essential thrombocythemia chronicled after the FDA approval date of anagrelide. *Am J Hematol*. 2019;94(1):5-9.